

# Semi-Supervised Co-Training of Time and Time-Frequency Models: Application to Bearing Fault Diagnosis

Tuomas Jalonen, Mohammad Al-Sa'd, *Senior Member, IEEE*, Serkan Kiranyaz, *Senior Member, IEEE*, and Moncef Gabbouj, *Fellow, IEEE*

**Abstract**—Neural networks require massive amounts of annotated data to train intelligent solutions. Acquiring many labeled data in industrial applications is often difficult; therefore, semi-supervised approaches are preferred. We propose a new semi-supervised co-training method, which combines time and time-frequency (TF) machine learning models to improve performance and reliability. The developed framework collaboratively co-trains fast time-domain models by utilizing high-performing TF techniques without increasing the inference complexity. Besides, it operates in cloud-edge networks and offers holistic support for many applications covering edge-real-time monitoring and cloud-based updates and corrections. Experimental results on bearing fault diagnosis verify the superiority of our technique compared to a competing self-training method. The results from two case studies show that our method outperforms self-training for different noise levels and amounts of available data with accuracy gains reaching from 10.6% to 33.9%. They demonstrate that fusing time-domain and TF-based models offers opportunities for developing high-performance industrial solutions.

## I. INTRODUCTION

NEURAL networks require extensive labeled data for supervised learning, where all data must be reliably annotated. Annotating data is challenging in many applications, especially fault diagnosis, as it can be labor-intensive, dangerous, or even impossible if faulty equipment is difficult to develop [1]. To address this, solutions based on semi-supervised, unsupervised learning, and domain adaptation have been developed [2], [3].

In semi-supervised learning, labeled and unlabeled data are combined [4], while unsupervised learning uses only unlabeled data [2]. Both approaches struggle with changes in data distribution, known as domain shift, common in fault diagnosis due to variations in operating conditions or environments. Domain adaptation addresses this issue by aligning distributions or adapting models trained on one domain (source) to perform on another (target) [3]. While domain adaptation transfers knowledge across domains, semi-supervised learning is more suitable with the personalized approach when labeled and unlabeled data share a consistent distribution.

A key semi-supervised approach is self-training, where a model initially trained with labeled data generates pseudo-labels for unlabeled data [5]. However, self-training can propagate errors, requiring monitoring or correction [6]. Another

method is co-training, where multiple models with different views of the data improve pseudo-labels collaboratively [7], [8]. For example, [9] used adversarial data to ensure classifier diversity in image recognition. Semi-supervised learning is highly relevant for fault diagnosis in machines like pumps, turbines, and motors. Bearings, a critical component, are prone to faults, but labeled vibration data can be scarce and costly to obtain [10], [11]. Consequently, semi-supervised learning leverages limited labeled data to enhance fault diagnosis.

Convolutional neural networks (CNNs) have been widely used for bearing fault diagnosis, leveraging one-dimensional (1D) time or frequency views [10], [12]–[14], and two-dimensional (2D) time-frequency (TF) representations [15]–[19]. TF-based CNNs often outperform 1D models, especially in noisy conditions [14], [16], but require significant computational resources. Transforming learned semantics from TF-CNNs to 1D-CNNs could reduce complexity while retaining accuracy.

Fusing different algorithms and data views can enhance decision systems' reliability and performance [20]. Fusion can be performed at the input, feature, or decision stages of model pipelines and implemented using various algorithms or auxiliary models [21]. TF models or classifiers improve decision-making fidelity by accessing and processing the signal's non-stationary dynamics [16], [22]. They achieve higher performance by leveraging a comprehensive joint time-frequency representation (TFR) [23]. However, the time-domain view remains valuable as it retains full temporal resolution, allowing machine learning algorithms to extract fine temporal features. We hypothesize that smart fusing or stacking of time-domain and TF models can lead to high-performance solutions with minimal computational overhead. Feature-level decision fusion with co-training was proposed in [24] for estimating the remaining useful life of bearings. This method showed acceptable performance but was limited to processing only 1D time and frequency views, excluding the richer TFR. Decision-level fusion can be achieved by combining the logits of multiple classifiers [25]. For example, [26] proposed semi-supervised collaborative learning, where pseudo-labels were generated by fusing decisions from two models, with confidence assessed via class-wise disagreement indicators. In [3], decision fusion was applied to domain adaptation for bearing fault diagnosis, but the models were constrained to 1D time-domain views.

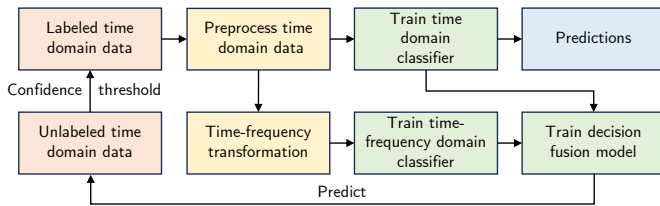


Fig. 1. The overall schematic of our proposed semi-supervised co-training method that combines the time and time-frequency models to generate more accurate and reliable predictions.

Similarly, predictions were fused using a weighted soft voting algorithm in [27] and mode-decomposition in [28], yet both approaches relied on limited time-domain representations. This highlights a significant knowledge gap in effectively fusing time-domain and TF-based machine learning models to develop high-performance semi-supervised solutions.

This paper proposes a semi-supervised co-training method that combines time-domain and TF-based classification models to improve performance and versatility in fault diagnosis. Unlike traditional domain adaptation approaches that address cross-domain discrepancies, this work assumes a consistent domain and focuses on leveraging complementary data representations to address annotation scarcity. The proposed method is particularly effective for scenarios where time and TF-based views provide distinct but complementary information, allowing for improved feature richness and decision reliability. In brief, our contributions are:

- 1) We propose a novel semi-supervised co-training method for time-series data by fusing time and TF-based machine learning models.
- 2) Experimental validation on two bearing fault datasets indicates that the proposed method offers gains in performance ranging from 10.5% up to 33%.
- 3) The proposed method is suitable for cloud-edge networks and offers holistic decentralized support for industrial applications covering real-time monitoring, scheduled model updates for higher performance, and fault record correction for better reliability.

The remainder of this paper is organized as follows: we explain our proposed method in section II, test its validity for two distinct bearing fault diagnosis problems in section III, and finally we conclude the paper in section IV.

## II. PROPOSED METHOD

The proposed semi-supervised co-training method is illustrated in Fig. 1. Our methodology assumes a practical case where a large set of collected data is available for classification purposes; however, only a small subset of these data samples is manually labeled. In other words, few data samples can be used directly for training in a supervised fashion, while the remaining cannot be naively used and require further preprocessing before utilization, i.e., semi-supervised learning. Besides, our technique fuses time- and TF-based classification models by co-training to improve their overall performance, reliability, and versatility.

### A. The Semi-Supervised Co-Training Technique

Our proposed semi-supervised co-training technique begins with preprocessing the labeled samples in the time domain and estimating their joint TF representation, generating two separate data views: a 1D time view and a 2D time-frequency view. Separate classifiers are trained in a supervised manner using each of these labeled data views. Additionally, a decision fusion model is trained using the outputs of these classifiers to enhance accuracy and robustness. Subsequently, the trained models are applied to a subset of the remaining unlabeled samples to generate pseudo-labeled predictions. These pseudo-labeled samples are incorporated into the original training set if the probability assigned to the class label exceeds a certain threshold, initiating a new training cycle. As training cycles progress, a greater number of unlabeled data is incorporated into the semi-supervised training process. Besides, the time and TF classifiers are co-trained by leveraging each other's advantages through the decision fusion model, which transfers the integrated semantics from the previous semi-supervised training cycle. This approach capitalizes on the fusion of both data views to minimize prediction errors and increase the system's reliability when applied to new data.

The main reasoning behind the proposed three-model structure is that TF transformation is computationally expensive. Hence, its corresponding model cannot operate in real-time or on edge devices. Therefore, we designed the proposed method so that it only relies on the fast time domain model when making predictions for new samples. Nevertheless, it benefits from both representation domains in the training phase to yield the best possible performance. This technique also offers a potential deployment strategy for cloud and edge devices where the co-training phase is solely performed on the cloud, while the real-time model is operated on edge devices. In the remainder of this section, we detail each component of the proposed methodology and discuss its potential deployment strategies for cloud and edge devices.

### B. Time Domain Preprocessing

Given a data acquisition system comprised of  $Q$  sensors, let  $s(t) = [s_1(t), s_2(t), \dots, s_Q(t)]^T$  be the set of measurements holding continuous stream of data, or signals, in a noisy environment, such that:

$$s_q(t) = v_q(t) + \alpha_q \eta_q(t), \quad (1)$$

where  $s_q(t)$  is the noisy signal or measurement recorded by sensor  $q$ ,  $v_q(t)$  is the unobserved clean measurement,  $\eta_q(t)$  is the measurement's noise, and  $\alpha_q$  is the noise degradation factor that defines the severity of noise deterioration, i.e.:

$$\alpha_q = 10^{-\text{SNR}/20} \sqrt{\frac{\int_0^T |v_q(t)|^2 dt}{\int_0^T |\eta_q(t)|^2 dt}}, \quad (2)$$

where  $T$  is the time duration of the measurement and SNR is the signal-to-noise ratio (SNR) in decibels (dB).

The acquired  $Q$  measurements are preprocessed in two stages, filtering and segmentation. First, we pass the signals through

a time-domain filter  $h(t)$  to reduce noise and to constrain the signals' spectra to a certain band for analysis, i.e.:

$$\mathbf{x}(t) = (h * \mathbf{s})(t) = \int_0^T h(\tau) \mathbf{s}(t - \tau) d\tau, \quad (3)$$

where  $\tau$  denotes temporal lag. After that, we partition the filtered signals into short segments of duration  $L$  with no overlap to yield manageable samples for training and testing. We express the segmented measurements as:  $[\mathbf{x}_1(t), \mathbf{x}_2(t), \dots, \mathbf{x}_P(t)]$ , where  $\mathbf{x}_p(t) = [x_{1,p}(t), x_{2,p}(t), \dots, x_{Q,p}(t)]^T$ ,  $p$  denotes the segment index, and  $P = T/L$  is the total number of segments.

### C. Time-Frequency Transformation

Let  $z_{q,p}(t)$  be the analytic associate of the segmented signal  $x_{q,p}(t)$  obtained via the Hilbert transform, such that:

$$z_{q,p}(t) = x_{q,p}(t) + j\mathcal{H}\{x_{q,p}(t)\}, \quad (4)$$

where  $\mathcal{H}\{\cdot\}$  is the Hilbert transform and  $j = \sqrt{-1}$ . The TFR of the signal, obtained by a TF distribution (TFD), illustrates the temporal evolution of its spectral content [23]. In other words, the TFR describes the signal's temporal and spectral information in a joint density-based representation, which reveals the signal's non-stationary dynamics that can help infer decisions about the signal under analysis [22]. The TFD of  $z_{q,p}(t)$  is expressed by:

$$\ell_{p,q}(t, f) = g_1(t) \underset{t}{*} W_{q,p}(t, f) \underset{f}{*} g_2(f), \quad (5)$$

$$W_{q,p}(t, f) = \int z_{q,p}\left(t + \frac{\tau}{2}\right) z_{q,p}^*\left(t - \frac{\tau}{2}\right) e^{-j2\pi\tau f} d\tau, \quad (6)$$

where  $\ell_{p,q}(t, f)$  is the smoothed TFD of  $z_{q,p}(t)$ ,  $W_{q,p}(t, f)$  is the Wigner-Ville distribution of  $z_{q,p}(t)$ ,  $g_1(t)$  and  $g_2(f)$  are separable time-domain and frequency-domain filters or kernels that control the resolution-accuracy trade-off in  $\ell_{p,q}(t, f)$  [22], respectively,  $\underset{t}{*}$  and  $\underset{f}{*}$  denote the convolution operation along the temporal and spectral axes, respectively, and  $z_{q,p}^*(t)$  is the complex conjugate of  $z_{q,p}(t)$ . This expression can be formulated in the Doppler-lag domain, a more convenient space where convolutions become multiplications [23], as:

$$\ell_{p,q}(t, f) = \iint G_1(\nu) A_{q,p}(\nu, \tau) G_2(\tau) e^{j2\pi(\nu t - \tau f)} d\tau d\nu, \quad (7)$$

$$A_{q,p}(\nu, \tau) = \int z_{q,p}\left(t + \frac{\tau}{2}\right) z_{q,p}^*\left(t - \frac{\tau}{2}\right) e^{-j2\pi t\nu} dt, \quad (8)$$

where  $\nu$  and  $\tau$  denote the Doppler and lag axes, respectively,  $G_1(\nu)$  and  $G_2(\tau)$  are the direct and inverse Fourier transforms of  $g_1(t)$  and  $g_2(f)$ , respectively, and  $A_{q,p}(\nu, \tau)$  is the ambiguity function of  $z_{q,p}(t)$ . In this work, we employ a compact kernel distribution (CKD) to estimate the TFR of the segmented signals because of its reported high TF accuracy, resolution, and overall effectiveness [22]. The CKD utilizes the following separable compact support kernels:

$$G_1(\nu) = \exp\left(c + \frac{cD^2}{\nu^2 - D^2}\right) : |\nu| < D, \quad (9)$$

$$G_2(\tau) = \exp\left(c + \frac{cE^2}{\tau^2 - E^2}\right) : |\tau| < E, \quad (10)$$

where  $D \in [0, 1]$  and  $E \in [0, 1]$  are the kernel normalized cut-offs along the Doppler and lag axes, respectively, and  $c > 0$  defines the shape of the kernel. We express the TFR of the segmented measurements as:  $[\ell_1(t, f), \ell_2(t, f), \dots, \ell_P(t, f)]$ , where  $\ell_p(t, f) = [\ell_{1,p}(t, f), \ell_{2,p}(t, f), \dots, \ell_{Q,p}(t, f)]^T$ .

### D. Time and Time-Frequency Domain Classifiers

We employ conventional time domain and TF domain CNN models [14], [16] for classification; however, our proposed semi-supervised co-training methodology is independent of the utilized classification techniques. Therefore, it should be noted that these employed models are just one example, and the proposed framework does not rely on CNNs by any means. For instance, the models could easily be replaced with more simple machine learning methods, such as K-Nearest Neighbors, or more sophisticated deep learning methods such as large language models, or any combination of them.

The utilized models in this work are based on the same five-layer CNN structure where all convolutional layers have 64 kernels with pool size and stride set to 2. The key differences between the time domain and the TF-CNN models are their 1D and 2D convolutions, respectively, and their input sizes which are set to  $(L \times f_s, Q)$  and  $(M \times f_s, M \times f_s, Q)$ , respectively, where  $f_s$  is the sampling frequency of the data acquisition system,  $M = \lambda \times L$ , and  $\lambda < 1$  is a down-sampling factor to reduce computational overheads. The convolutional layers in each model are followed by a dropout layer, a fully connected layer with 128 nodes, a ReLU activation function, another dropout, and a final classification layer of  $N$  nodes with softmax activation where  $N$  is the total number of classes to be predicted.

### E. Decision Fusion Model

Let  $\mathcal{M}_t$  and  $\mathcal{M}_{tf}$  be functions representing the time and the TF domain classification models, respectively. The predictions of the models can be expressed as follows:

$$\hat{\mathcal{Y}}_t = \mathcal{M}_t([\mathbf{x}_1(t), \mathbf{x}_2(t), \dots, \mathbf{x}_P(t)]), \quad (11)$$

$$\hat{\mathcal{Y}}_{tf} = \mathcal{M}_{tf}([\ell_1(t, f), \ell_2(t, f), \dots, \ell_P(t, f)]), \quad (12)$$

where  $\hat{\mathcal{Y}}_t$  and  $\hat{\mathcal{Y}}_{tf}$  are  $N \times P$  matrices holding the normalized logits from the time-domain and the TF classification models for all input segments, respectively. We fuse the predictions of the time and TF classifiers by summing their normalized logits in a weighted fashion, i.e.:

$$\hat{\mathcal{Y}}_{\text{fused}} = (\beta_t^T \times \mathbf{1}_P) \times \hat{\mathcal{Y}}_t + (\beta_{tf}^T \times \mathbf{1}_P) \times \hat{\mathcal{Y}}_{tf}, \quad (13)$$

where  $\hat{\mathcal{Y}}_{\text{fused}}$  holds the fused logits for all segments,  $\mathbf{1}_P = [1, 1, \dots, 1] \in \mathbb{R}^P$ ,  $\beta_t = [\beta_{t,1}, \beta_{t,2}, \dots, \beta_{t,N}]$  and  $\beta_{tf} = [\beta_{tf,1}, \beta_{tf,2}, \dots, \beta_{tf,N}]$  hold the optimal fusion weights of the time-domain and TF models, respectively, for each class. We compute the optimal fusion weights by minimizing the sum of squared errors between the predictions and their true counterparts. Specifically, the fusion weights for class  $n$  predictions are calculated as follows:

$$[\beta_{t,n}, \beta_{tf,n}]^T = (\hat{\mathcal{Y}}_n \hat{\mathcal{Y}}_n^T)^{-1} \hat{\mathcal{Y}}_n \mathcal{Y}_n^T, \quad (14)$$

where  $\hat{\mathcal{Y}}_n = [\hat{\mathcal{Y}}_{t,n}, \hat{\mathcal{Y}}_{tf,n}]^T$  holds the normalized logits for class  $n$  from each individual model,  $\mathcal{Y}$  is an  $N \times P$  matrix holding the true one-hot-encoded labels for all segments, and  $\mathcal{Y}_n$  is its  $n$ th row denoting the true binary labels for class  $n$ . Finally, we standardize  $\hat{\mathcal{Y}}_{\text{fused}}$  to strictly hold positive values with columns summing up to one, and compute the system's fused decisions for every input segment as follows:

$$\hat{\mathbf{y}} = \arg \max_n \left( \hat{\mathcal{Y}}_{\text{fused}} \right), \quad (15)$$

where  $\hat{\mathbf{y}} = [\hat{y}_1, \hat{y}_2, \dots, \hat{y}_P]$  hold the predicted classes that will be compared to the true ones in  $\mathbf{y}$  to quantify performance.

### F. Confidence Thresholding

We design a confidence thresholding mechanism to ensure that only reliable pseudo-labeled samples are included in the retraining process and to maintain class balance. Specifically, given the set of all available samples  $\mathcal{D}$ , we find a set  $\mathcal{S} \subseteq \mathcal{D}$  holding samples with reliable predictions for each class  $n$ :

$$\mathcal{S} = \{\mathcal{S}_1, \mathcal{S}_2, \dots, \mathcal{S}_N\}, \quad (16)$$

where  $\mathcal{S}_n$  is the subset of samples holding time and TF pairs that yield high-value logits for class  $n$ , i.e.:

$$\mathcal{S}_n = \left\{ \{x_p(t), \ell_p(t, f)\} : \max_n \left( \hat{\mathcal{Y}}_{\text{fused}, p} \right) > \xi, \forall p \in [1, P] \right\}, \quad (17)$$

where  $\xi$  is a user-defined confidence, or logits, threshold. To ensure balance between the number of samples in each class, the subsets are computed subject to the following criterion:

$$\#(\mathcal{S}_n) = \frac{1}{N} \sum_{n=1}^N \#(\mathcal{S}_n). \quad (18)$$

### G. Deployment Strategy for Cloud and Edge Devices

The time-domain CNN model was reported to operate in real-time even on low-cost edge devices [14]. This is due to its minimal memory footprint, small input size, and simple preprocessing procedures. In contrast, the TF model is known to be a non-real-time solution because of its high number of parameters, large input size, and computationally expensive data transformation process [16]. Therefore, we offer a potential deployment strategy for our proposed semi-supervised co-training method in cloud-edge networks where the co-training phase is solely performed in the cloud or a local server, while the real-time prediction phase is conducted on the edge device(s); see the schematic in Fig. 2.

Initially, all three classifiers are trained in the cloud or the local server in a supervised manner by holding out a testing set. After that, a copy of the trained time-domain classifier is sent out to all edge devices for real-time inference. We keep a copy of this trained classifier in the cloud and refer to it as the original time-domain model. Then, edge devices send back the new unlabeled samples to the cloud or server to conduct the proposed semi-supervised co-training procedure. Note that this procedure does not require fast communication and can be initiated whenever a sufficient amount of unlabeled data is received. We compare the newly updated (co-trained) time-domain model to its original version using the held-out

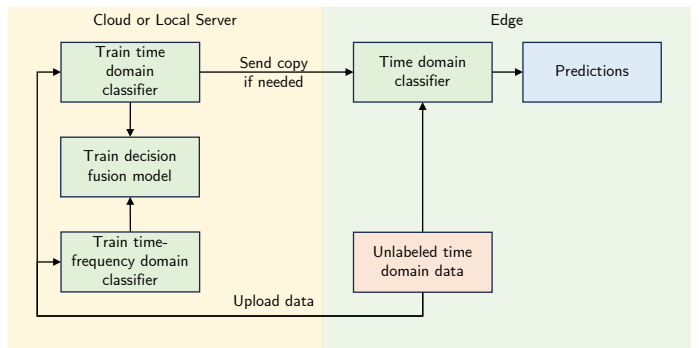


Fig. 2. The schematic of our proposed semi-supervised co-training method deployed on a cloud-edge network.

testing set. If we detect a considerable performance gain, the updated co-trained time-domain model is sent out to replace its original version. Additionally, the fused non-real-time model in the cloud or server can be used to correct the prediction log on each edge device. However, the continuous dependence on this service can be decided by the end-user. In other words, the end-user has three options: (1) operate offline by utilizing the originally trained fast model with no updates, (2) permit scheduled updates for the fast time-domain model from the server, and (3) permit full support from both the edge device and the cloud service which includes: real-time monitoring, scheduled model updates for higher performance, and fault record correction via the fused non-real-time model for better reliability. This proposed framework enables faster fault detection, more reliable predictions, lower energy consumption which makes battery operation feasible, and lower hardware costs compared to using one large model either in the cloud or on the edge device. In brief, our proposed method and its deployment strategy can fuse the best parts of the two domains: the high accuracy from the TF-domain model and the faster predictions from the time-domain model.

## III. EXPERIMENTAL VALIDATIONS

The validity of our hypothesized method is tested by applying it to the problem of bearing fault diagnosis under time-varying speeds and variable noise levels. The overview of the proposed method within the bearing fault diagnosis problem is shown in Fig. 3. Specifically, we conduct two case studies to determine if the proposed semi-supervised co-training method can yield consistent reliable predictions across different variables; see Table I. Besides we compare it to another semi-supervised training technique to quantify its possible gains in performance and robustness.

### A. Case Studies and Preprocessing

1) *Case study KAIST*: This experiment uses vibration signals to diagnose bearing faults under rapidly varying motor speeds. We used an open-access dataset from the Korean Advanced Institute of Science and Technology (KAIST) [29], which includes four classes: *Normal*, *Outer*, *Inner*, and *Ball*, describing a typical bearing function and three common faults. For each of these classes, 35 minutes of vibration data were

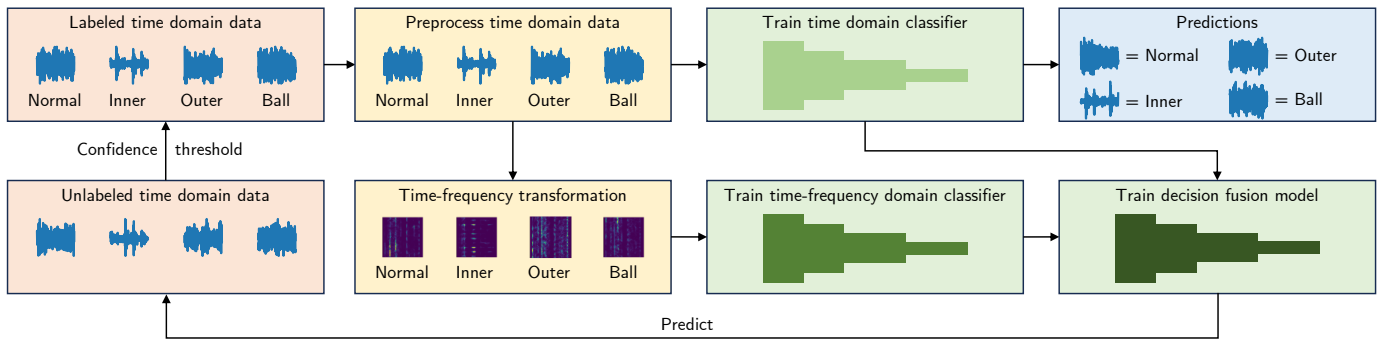


Fig. 3. The schematic of our proposed semi-supervised co-training method for the bearing fault diagnosis application. The number of classes and labels come from the KAIST case study as an example of the utility of our method.

acquired using two accelerometers installed on the x- and y-axes of the bearing housing. The signals were originally sampled at 25.6 kHz, but we downsampled them to 20 kHz using a Finite Impulse Response (FIR) anti-aliasing lowpass filter with delay compensation. Additionally, we partitioned the filtered signals into 100 ms segments and added white Gaussian noise at various SNR levels. Finally, we computed the TFR of the segmented measurements using the CKD and downsampled their TF representations.

2) *Case study SQV*: This experiment includes diagnosing the severity of bearing faults under well-defined time-varying speeds using vibration signals. We used the publicly available Spectra Quest Vibration (SQV) dataset which includes seven classes: *Normal*, *Outer 1*, *Outer 2*, *Outer 3*, *Inner 1*, *Inner 2*, and *Inner 3* [30]. This dataset describes a typical bearing function and two common faults with three degrees of severity: 1 is mild, 2 is moderate, and 3 indicates a severe fault condition. For each of these classes, 2.7 minutes, on average, of vibration data were acquired using one accelerometer. These measurements were made under a continuously varying motor speed set to increase from rest to 3000 rpm, stay at 3000 rpm for a while, and then continuously decelerate to rest again. We linearly interpolated the measured speed to match the temporal sampling of the vibration signals at 25.6 kHz. Besides, we automatically extracted regions of interest corresponding to periods when the speed was significantly non-zero (on average above 200 rpm). This process resulted in reducing the duration of the vibration signals to 1.84 minutes on average. After that, we partitioned the vibration signals into 78.125 ms segments and added white Gaussian noise at various SNR levels. Note that there was a class imbalance problem, which we solved by selecting the first 1300 segments from each class and discarding the rest. Finally, we computed and downsampled the TFR of the remaining segments similarly to the first case study.

**B. Competing Method and Experimental Settings**

1) *Self-training*: We compare our semi-supervised co-training method against the self-training technique in Fig. 4 to quantify any performance gains. The main difference to our technique is that, in self-training, the time-domain classifier is re-trained by feeding back its pseudo-labeled predictions.

TABLE I  
THE PRE-PROCESSING PARAMETERS FOR THE TWO CASE STUDIES.

Parameters	Case Study KAIST	Case Study SQV
$N$	4 classes	7 classes
$Q$	2 sensors	2 sensors
$T$	35 min per sensor per class	$\approx 2.7$ min per sensor per class
$L$	100 ms	78.125 ms
$P$	21,000 segments per sensor per class	$\approx 1,407$ segments per sensor per class
$f_s$	20 kHz	25.6 kHz
$h(t)$	FIR lowpass filter with delay compensation	—
SNR	$\{-5, 0, 5\}$ dB	$\{-5, 0, 5\}$ dB
$\lambda$	0.064	0.064
$\{c, D, E\}$	$\{1, 0.1, 0.1\}$	$\{1, 0.1, 0.1\}$

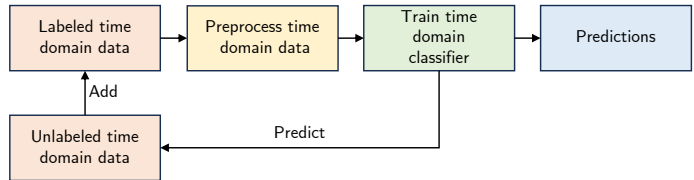


Fig. 4. The schematic of the comparative self-training method.

2) *Training and testing setups*: We divided the datasets into ten equal temporal splits. We used the first split, which is 10% of all data, in the initial supervised training with ground truth labels, held out the last two splits for testing, and utilized the remaining seven splits in the semi-supervised training with pseudo-labels. We also fixed the structures and hyperparameters of all models regardless of the noise level or case study ( $10^{-5}$  learning rate; 0.8 confidence threshold). However, the batch sizes (SQV: 10, KAIST: 100), and the number of epochs (SQV: 100, KAIST: 80) were different. At the initial supervised training phase, weights of the time-domain and TF classification models were initialized randomly. These weights were also used to initialize the models during the first semi-supervised self-training and co-training

phases to ensure fair and consistent learning scenarios in the beginning. After the supervised training phase, the trained decision fusion model was applied to the first unlabeled data split to generate pseudo-labels. These pseudo-labeled samples were incorporated into the training set and used to retrain all three models if the probability assigned to the class label exceeded the confidence threshold. This process was repeated for all the seven unlabeled data splits. Finally, we measured the models' classification performance at different stages via the held-out testing set, and we repeated this entire process four times to ensure consistency, reliability, and the results' significance.

### C. Results and Discussion

Table II demonstrates the testing performance of the initial supervised time-domain model. It reports the testing accuracy at different SNR levels and for the two case studies; KAIST and SQV. The results show that accuracy inversely correlates with the SNR level and that performance on the SQV dataset is more affected by noise. However, the accuracy is slightly decreased with KAIST when moving from 5 dB to clean, which is counterintuitive. The phenomenon is not present with SQV. Specifically, the accuracy difference between clean and -5 dB is almost four times higher than the KAIST's. Besides, the accuracy on SQV at -5 dB is only 43% when compared to the 64% for KAIST. This perhaps is due to the smaller number of samples in the SQV dataset and its higher number of classes. Nevertheless, these results only act as baselines for the semi-supervised outcomes to help us quantify any gains in performance.

Table III presents the testing performance of the proposed semi-supervised co-training method and compares it to the competing self-training technique. The table summarizes the testing accuracy for the two case studies, at different SNR levels, and across the increasing number of unlabeled training samples. On the one hand, by analyzing the results across the different SNR levels, one notes that the performance of both the co-training and self-training algorithms increases at higher SNR levels. However, the performance on the clean KAIST data decreases from 5 dB similar to the initial supervised models. On the other hand, by examining the trends across the increasing number of unlabeled training samples, we find that the testing scores for the self-training technique are practically unchanged, while remarkably increasing for the proposed co-training method. In fact, the proposed co-training method achieves higher performance than the comparative self-training technique in both case studies and across all variables; noise levels and number of unlabeled training samples. For instance, it reaches 83% (KAIST) and 90% (SQV) accuracy when supplied with clean signals in both case studies compared to only 74% and 75% for the self-training method. But what stands out in the table is that the proposed co-training method reaches 75% at -5 dB (KAIST), while the self-training technique barely reaches 74% when supplied with clean vibration signals. This demonstrates the versatility of our method even at such severe noise levels.

Figs. 5 and 6 further examine the gain in performance delivered by the proposed co-training method. In Fig. 5, the

testing accuracy, when using all the unlabeled training data, is illustrated with bar plots across the different noise levels and for the two case studies. The results also demonstrate the accuracy's 95% confidence interval and the relative gains delivered by our proposed method. By inspecting the accuracy bars, it becomes apparent that our co-training method outperforms the self-training technique across all noise levels. But more importantly, the results verify its consistent relative boost in performance ranging from 10.6% up to 17.2% (13.6% on average) for the KAIST dataset and from 19.8% up to 33.9% (23.2% on average) for the SQV case; see Figs. 5a and 5b. Moreover, Fig. 6 expands this comparison by displaying the relationship between the averaged testing accuracy and the number of training samples for the clean case. The reported trends reveal that the semi-supervised self-training technique did not benefit from the increase in the number of unlabeled training samples. Specifically, it demonstrates a statistically flat performance profile for the KAIST and SQV datasets; see Figs. 6a and 6. In contrast, our proposed semi-supervised co-training method offers major gains in performance that are positively correlated with the amount of supplied data. In other words, it achieves higher accuracy given more unlabeled training samples. Furthermore, the results show an upward trend for the co-training performance in both case studies. This implies that the final accuracy could be even higher if more unlabeled training data was available. Nonetheless, the standard deviation of the co-training model also increases towards the end, at least in the KAIST case study.

## IV. CONCLUSIONS

This paper presented a novel semi-supervised co-training method that combines time and time-frequency (TF) based machine learning models to improve performance and reliability. The proposed fusion was motivated by the scarcity of labeled data in many industrial applications and by the trade-off in performance and computational complexity, where the TF view offers more relevant features but adds significant computational overhead. Therefore, we developed a framework that utilizes the learned TF semantics to co-train a fast time-domain model in a collaborative semi-supervised manner without any increase in inference complexity. Besides, we showed that the proposed methodology is suitable for cloud-edge networks and offers holistic decentralized support for many industrial applications covering real-time monitoring, scheduled model updates for higher performance, and fault record correction for better reliability.

The validity of our semi-supervised co-training method was tested by applying it to the problem of bearing fault diagnosis under time-varying speeds and variable noise levels. We conducted two case studies to determine if the proposed method can yield consistent reliable predictions across different variables. In addition, we compared it to a competing self-training semi-supervised technique for different noise levels and amounts of available training data. In brief, the experimental results demonstrated that the proposed co-training method outperforms the self-training technique in both case studies, across all noise levels, and for any amount of available

TABLE II

THE INITIAL SUPERVISED LEARNING RESULTS IN THE TIME DOMAIN MODEL FOR THE TWO CASE STUDIES IN TERMS OF THE TESTING SET ACCURACY SCORES  $\pm$  STANDARD DEVIATIONS ACROSS THE DIFFERENT SNR LEVELS. THE MODELS WERE TRAINED WITH THE FIRST 10% OF THE DATA USING GROUND-TRUTH LABELS.

Case Study	# Labeled Training Samples	The Samples Temporal Span	SNR = -5 dB	SNR = 0 dB	SNR = 5 dB	Clean
KAIST	8.4k	0 – 3.5 min	64.24 $\pm$ 0.29	69.06 $\pm$ 0.51	73.44 $\pm$ 0.37	73.23 $\pm$ 0.23
SQV	0.9k	0 – 71 sec	42.83 $\pm$ 1.48	59.67 $\pm$ 0.86	67.54 $\pm$ 0.39	73.98 $\pm$ 0.21

TABLE III

THE SEMI-SUPERVISED SELF-TRAINING AND CO-TRAINING RESULTS FOR THE TWO CASE STUDIES. THE RESULTS ARE SUMMARIZED BY THE TESTING SET ACCURACY SCORES AVERAGED OVER FOUR REPETITIONS  $\pm$  STANDARD DEVIATIONS. THE BEST RESULTS ARE HIGHLIGHTED IN BOLD ACROSS THE DIFFERENT SNR LEVELS AND THE NUMBER OF UNLABELED TRAINING SAMPLES.

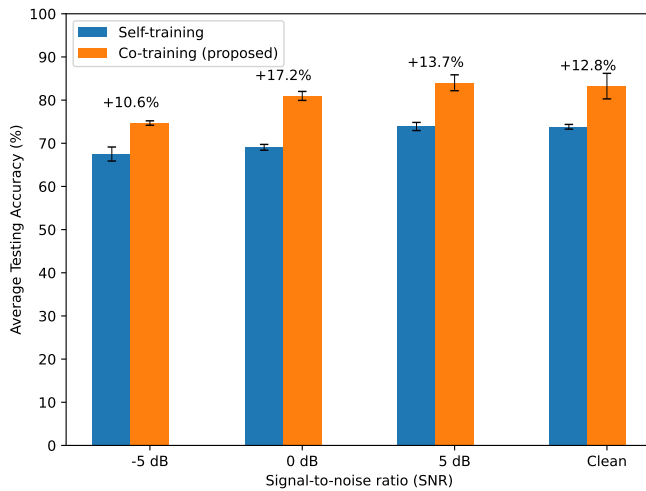
Case Study	# Unlabeled Training Samples	The Samples Temporal Span	SNR = -5 dB		SNR = 0 dB		SNR = 5 dB		Clean	
			Self-Training	Co-Training	Self-Training	Co-Training	Self-Training	Co-Training	Self-Training	Co-Training
KAIST	8.4k	3.5–7.0 min	66.59 $\pm$ 0.49	<b>68.25 <math>\pm</math> 0.35</b>	68.57 $\pm$ 0.67	<b>72.90 <math>\pm</math> 0.11</b>	73.19 $\pm$ 0.56	<b>74.00 <math>\pm</math> 0.46</b>	73.58 $\pm$ 0.28	<b>75.28 <math>\pm</math> 0.28</b>
	16.8k	3.5–10.5 min	66.55 $\pm$ 0.37	<b>70.95 <math>\pm</math> 0.42</b>	69.22 $\pm$ 0.43	<b>75.94 <math>\pm</math> 0.07</b>	73.41 $\pm$ 0.22	<b>77.10 <math>\pm</math> 0.38</b>	73.64 $\pm$ 0.31	<b>78.91 <math>\pm</math> 0.32</b>
	25.2k	3.5–14.0 min	67.50 $\pm$ 0.14	<b>72.16 <math>\pm</math> 0.15</b>	69.29 $\pm$ 0.49	<b>77.69 <math>\pm</math> 0.25</b>	73.74 $\pm$ 0.43	<b>80.55 <math>\pm</math> 0.47</b>	73.82 $\pm$ 0.12	<b>80.91 <math>\pm</math> 1.53</b>
	33.6k	3.5–17.5 min	67.16 $\pm$ 0.80	<b>73.12 <math>\pm</math> 0.36</b>	68.56 $\pm$ 0.47	<b>79.48 <math>\pm</math> 0.28</b>	73.90 $\pm$ 0.39	<b>82.37 <math>\pm</math> 0.36</b>	73.97 $\pm$ 0.22	<b>81.41 <math>\pm</math> 1.13</b>
	42.0k	3.5–21.0 min	67.22 $\pm$ 0.71	<b>73.54 <math>\pm</math> 0.90</b>	68.71 $\pm$ 0.55	<b>80.42 <math>\pm</math> 0.22</b>	73.53 $\pm$ 0.58	<b>83.58 <math>\pm</math> 0.32</b>	73.74 $\pm$ 0.17	<b>82.09 <math>\pm</math> 1.33</b>
	50.4k	3.5–24.5 min	67.24 $\pm$ 0.66	<b>74.03 <math>\pm</math> 0.48</b>	69.24 $\pm$ 0.36	<b>80.92 <math>\pm</math> 0.31</b>	73.20 $\pm$ 0.56	<b>83.83 <math>\pm</math> 1.11</b>	73.93 $\pm$ 0.17	<b>82.59 <math>\pm</math> 1.45</b>
	58.8k	3.5–28.0 min	67.51 $\pm$ 0.83	<b>74.69 <math>\pm</math> 0.26</b>	69.07 $\pm$ 0.34	<b>80.97 <math>\pm</math> 0.53</b>	73.89 $\pm$ 0.48	<b>84.02 <math>\pm</math> 0.94</b>	73.82 $\pm$ 0.28	<b>83.24 <math>\pm</math> 1.51</b>
SQV	0.9k	71–142 sec	45.78 $\pm$ 2.05	<b>49.53 <math>\pm</math> 1.92</b>	60.52 $\pm$ 0.79	<b>61.59 <math>\pm</math> 0.83</b>	68.09 $\pm$ 0.38	<b>70.66 <math>\pm</math> 0.58</b>	74.08 $\pm$ 0.11	<b>79.20 <math>\pm</math> 0.32</b>
	1.8k	71–213 sec	46.81 $\pm$ 1.22	<b>55.81 <math>\pm</math> 0.58</b>	60.58 $\pm$ 0.87	<b>65.33 <math>\pm</math> 0.61</b>	68.43 $\pm$ 0.39	<b>74.78 <math>\pm</math> 0.45</b>	74.38 $\pm$ 0.27	<b>82.72 <math>\pm</math> 0.64</b>
	2.7k	71–284 sec	46.40 $\pm$ 1.62	<b>57.61 <math>\pm</math> 0.59</b>	61.63 $\pm$ 0.48	<b>69.57 <math>\pm</math> 0.55</b>	68.34 $\pm$ 0.32	<b>78.19 <math>\pm</math> 0.47</b>	74.31 $\pm$ 0.45	<b>84.26 <math>\pm</math> 0.14</b>
	3.6k	71–355 sec	47.10 $\pm$ 1.83	<b>60.95 <math>\pm</math> 0.36</b>	61.06 $\pm$ 0.73	<b>71.55 <math>\pm</math> 0.20</b>	68.75 $\pm$ 0.25	<b>79.85 <math>\pm</math> 0.37</b>	74.85 $\pm$ 0.51	<b>86.80 <math>\pm</math> 0.58</b>
	4.6k	71–427 sec	46.74 $\pm$ 1.04	<b>61.48 <math>\pm</math> 1.24</b>	61.80 $\pm$ 0.80	<b>72.75 <math>\pm</math> 0.62</b>	68.86 $\pm$ 0.32	<b>80.27 <math>\pm</math> 0.59</b>	74.82 $\pm$ 0.37	<b>87.97 <math>\pm</math> 0.66</b>
	5.5k	71–498 sec	46.83 $\pm$ 1.82	<b>63.32 <math>\pm</math> 0.47</b>	61.29 $\pm$ 1.08	<b>72.39 <math>\pm</math> 0.68</b>	68.65 $\pm$ 0.27	<b>81.44 <math>\pm</math> 0.67</b>	74.22 $\pm$ 0.49	<b>89.07 <math>\pm</math> 0.76</b>
	6.4k	71–569 sec	47.45 $\pm$ 1.38	<b>63.52 <math>\pm</math> 0.39</b>	61.37 $\pm$ 0.57	<b>73.50 <math>\pm</math> 0.38</b>	69.09 $\pm$ 0.72	<b>82.07 <math>\pm</math> 0.68</b>	74.70 $\pm$ 0.54	<b>89.78 <math>\pm</math> 0.08</b>

training data. Additionally, they showed that our method offers major gains in accuracy, starting from 10.6% up to 33.9%, without any added inference complexity. Consequently, the experimental results verify that fusing time domain and TF-based machine learning models offers new opportunities for developing high-performance semi-supervised solutions.

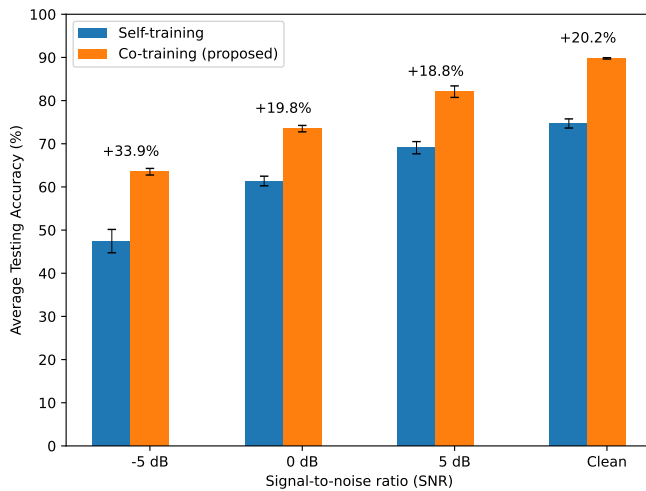
This work has focused on the motor fault diagnosis application, but it is interesting to see how the proposed method would perform on other semi-supervised time-series classification, regression or domain adaptation problems. The classification models utilized in this paper are simple, albeit effective, and more sophisticated techniques, such as large language models, could improve the performance of our method even further. Our work could also benefit from employing transfer learning techniques and optimizing the TF representations. Addressing these shortcomings will be our focus in the future.

## REFERENCES

- [1] X. Chen, R. Yang, Y. Xue, M. Huang, R. Ferrero, and Z. Wang, “Deep transfer learning for bearing fault diagnosis: A systematic review since 2016,” *IEEE Transactions on Instrumentation and Measurement*, 2023.
- [2] G.-J. Qi and J. Luo, “Small data challenges in big data era: A survey of recent progress on unsupervised and semi-supervised methods,” *IEEE Transactions on Pattern Analysis and Machine Intelligence*, vol. 44, no. 4, pp. 2168–2187, 2020.
- [3] T. Gao, J. Yang, and Q. Tang, “A multi-source domain information fusion network for rotating machinery fault diagnosis under variable operating conditions,” *Information Fusion*, p. 102278, 2024.
- [4] X. Yang, Z. Song, I. King, and Z. Xu, “A survey on deep semi-supervised learning,” *IEEE Transactions on Knowledge and Data Engineering*, vol. 35, no. 9, pp. 8934–8954, 2022.
- [5] S. Zheng and J. Zhao, “A self-adaptive temporal-spatial self-training algorithm for semisupervised fault diagnosis of industrial processes,” *IEEE transactions on industrial informatics*, vol. 18, no. 10, pp. 6700–6711, 2021.
- [6] Y. Chen, M. Mancini, X. Zhu, and Z. Akata, “Semi-supervised and unsupervised deep visual learning: A survey,” *IEEE transactions on pattern analysis and machine intelligence*, vol. 46, no. 3, pp. 1327–1347, 2022.
- [7] A. Blum and T. Mitchell, “Combining labeled and unlabeled data with co-training,” in *Proceedings of the eleventh annual conference on Computational learning theory*, 1998, pp. 92–100.
- [8] X. Ning, X. Wang, S. Xu, W. Cai, L. Zhang, L. Yu, and W. Li, “A review of research on co-training,” *Concurrency and computation*, vol. 35, no. 18, 2023.
- [9] S. Qiao, W. Shen, Z. Zhang, B. Wang, and A. Yuille, “Deep co-training for semi-supervised image recognition,” in *Proceedings of the european conference on computer vision (eccv)*, 2018, pp. 135–152.
- [10] H. Wang, Z. Liu, D. Peng, and Y. Qin, “Understanding and learning discriminant features based on multiattention 1denn for wheelset bearing fault diagnosis,” *IEEE Transactions on Industrial Informatics*, vol. 16, no. 9, pp. 5735–5745, 2019.
- [11] S. Zhang, S. Zhang, B. Wang, and T. G. Habetler, “Deep learning algorithms for bearing fault diagnostics—a comprehensive review,” *IEEE Access*, vol. 8, pp. 29 857–29 881, 2020.
- [12] L. Wang, Y. Gao, X. Li, and L. Gao, “Self-supervised-enabled open-set cross-domain fault diagnosis method for rotating machinery,” *IEEE Transactions on Industrial Informatics*, 2024.
- [13] Z. Tang, Z. Su, S. Wang, M. Luo, H. Luo, and L. Bo, “Fault diagnosis of rotating machinery toward unseen working condition: A regularized domain adaptive weight optimization,” *IEEE Transactions on Industrial Informatics*, 2024.
- [14] T. Jalonen, M. Al-Sa’d, S. Kiranyaz, and M. Gabbouj, “Real-time vibration-based bearing fault diagnosis under time-varying speed conditions,” in *2024 IEEE International Conference on Industrial Technology (ICIT)*. IEEE, 2024, pp. 1–7.
- [15] Z. Shi, J. Chen, Y. Zi, and Z. Zhou, “A novel multitask adversarial network via redundant lifting for multicomponent intelligent fault detection under sharp speed variation,” *IEEE Transactions on Instrumentation and Measurement*, vol. 70, pp. 1–10, 2021.
- [16] M. Al-Sa’d, T. Jalonen, S. Kiranyaz, and M. Gabbouj, “Quadratic time-frequency analysis of vibration signals for diagnosing bearing faults,” *arXiv preprint arXiv:2401.01172*, 2024.
- [17] Y. Qu, X. Wang, X. Zhang, and S. Huang, “An adaptive method for multifault diagnosis of induction motor under sharp changing speed and load condition,” *IEEE Transactions on Industrial Informatics*, 2023.

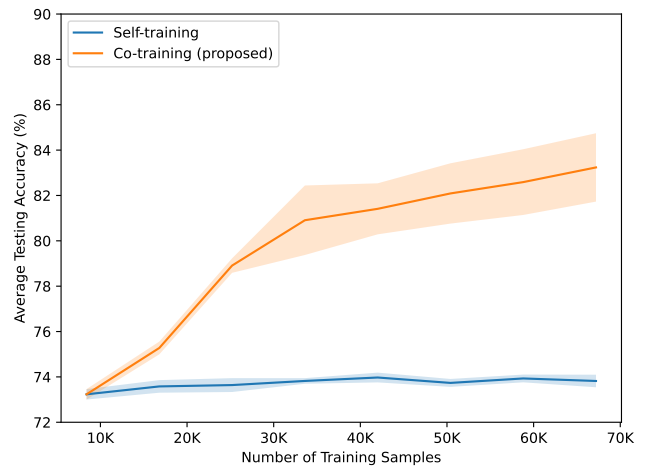


(a) Testing performance using the KAIST dataset.

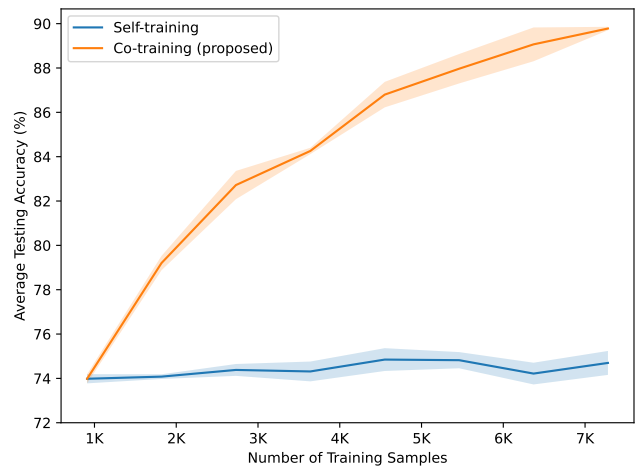


(b) Testing performance using the SQV dataset.

Fig. 5. The testing accuracy of the self-training and the proposed co-training semi-supervised techniques. Averaged results are depicted across the different SNR levels along with their corresponding 95% confidence intervals and relative gains in performance.



(a) Case study: KAIST.



(b) Case study: SQV.

Fig. 6. The relationship between the number of training samples and the testing performance for the semi-supervised self-training and the co-training techniques. The results show the averaged testing accuracy  $\pm$  standard deviation when utilizing the clean data in each case study.

- [18] Y. Deng, D. Huang, S. Du, G. Li, C. Zhao, and J. Lv, "A double-layer attention based adversarial network for partial transfer learning in machinery fault diagnosis," *Computers in Industry*, vol. 127, p. 103399, 2021.
- [19] D. B. Verstraete, E. L. Droguett, V. Meruane, M. Modarres, and A. Ferrada, "Deep semi-supervised generative adversarial fault diagnostics of rolling element bearings," *Structural Health Monitoring*, vol. 19, no. 2, pp. 390–411, 2020.
- [20] M. A. Ganaie, M. Hu, A. K. Malik, M. Tanveer, and P. N. Suganthan, "Ensemble deep learning: A review," *Engineering Applications of Artificial Intelligence*, vol. 115, p. 105151, 2022.
- [21] T. Meng, X. Jing, Z. Yan, and W. Pedrycz, "A survey on machine learning for data fusion," *Information Fusion*, vol. 57, pp. 115–129, 2020.
- [22] M. Al-Sa'd, B. Boashash, and M. Gabbouj, "Design of an Optimal Piece-Wise Spline Wigner-Ville Distribution for TFD Performance Evaluation and Comparison," *IEEE Transactions on Signal Processing*, vol. 69, pp. 3963–3976, 2021.
- [23] B. Boashash, Ed., *Time-Frequency Signal Analysis and Processing*, 2nd ed. Oxford: Academic Press, 2016.
- [24] X. Yan, X. Xia, L. Wang, and Z. Zhang, "A cotraining-based semisupervised approach for remaining-useful-life prediction of bearings," *Sensors*, vol. 22, no. 20, p. 7766, 2022.
- [25] Q. Guo, X. Wang, Y. Wu, Z. Yu, D. Liang, X. Hu, and P. Luo, "Online knowledge distillation via collaborative learning," in *Proceedings of the IEEE/CVF Conference on Computer Vision and Pattern Recognition*, 2020, pp. 11 020–11 029.
- [26] S. Fan, F. Zhu, Z. Feng, Y. Lv, M. Song, and F.-Y. Wang, "Conservative-progressive collaborative learning for semi-supervised semantic segmentation," *IEEE Transactions on Image Processing*, 2023.
- [27] Z. Xu, M. Bashir, W. Zhang, Y. Yang, X. Wang, and C. Li, "An intelligent fault diagnosis for machine maintenance using weighted soft-voting rule based multi-attention module with multi-scale information fusion," *Information Fusion*, vol. 86, pp. 17–29, 2022.
- [28] A. Yang, M. Wu, C. Lu, W. Yu, J. Hu, and Y. Nakanishi, "Decision fusion scheme based on mode decomposition and evidence theory for fault diagnosis of drilling process," *IEEE Transactions on Industrial Informatics*, 2023.
- [29] W. Jung, S.-H. Kim, S.-H. Yun, J. Bae, and Y.-H. Park, "Vibration, acoustic, temperature, and motor current dataset of rotating machine under varying operating conditions for fault diagnosis," *Data in brief*, vol. 48, pp. 109 049–109 049, 2023.
- [30] S. Liu, J. Chen, S. He, Z. Shi, and Z. Zhou, "Subspace network with shared representation learning for intelligent fault diagnosis of machine under speed transient conditions with few samples," *ISA transactions*, vol. 128, pp. 531–544, 2022.